# Precise Modulation of $CO_2$ Sorption in $Ti_8Ce_2$ -Oxo Clusters: Elucidating Lewis Acidity of the Ce Metal Sites and Structural Flexibility

Xingjie Wang, \*,#, a Haomiao Xie, #,b Debabrata Sengupta, b Fanrui Sha, b Ken-ichi Otake, d Yongwei Chen, b Karam B. Idrees, b Kent O. Kirlikovali, b Florencia Son, b Meng Wang, d Junli Ren, a Justin M. Notestein, c Susumu Kitagawa, \*,d Omar K. Farha\*, b, c

- <sup>a</sup> State Key Laboratory of Pulp and Paper Engineering, School of Light Industry and Engineering, South China University of Technology, Guangzhou 510640, China
- <sup>b</sup> International Institute for Nanotechnology and Department of Chemistry, Northwestern University, 2145 Sheridan Road, Evanston, Illinois 60208, United States
- <sup>c</sup> Department of Chemical and Biological Engineering, Northwestern University, 2145 Sheridan Road, Evanston, Illinois 60208, United States
- <sup>d</sup> Institute for Integrated Cell-Material Sciences, Kyoto University Institute for Advanced Study, Kyoto University, Yoshida Ushinomiya-cho, Sakyo-ku, Kyoto 606-8501, Japan.
- # These authors contribute equally to this work.

\*Corresponding author: Xingjie Wang, Susumu Kitagawa, Omar K. Farha, Email: xingjiewang1210@scut.edu.cn, kitagawa@icems.kyoto-u.ac.jp, o-farha@northwestern.edu

**KEYWORDS:** Flexible metal oxide cluster; bimetallic metal oxide cluster; titanium-cerium oxo cluster; stepped sorption behavior; in-situ SCXRD

**ABSTRACT:** The quest for understanding the structure-property correlation in porous materials has remained a persistent focus across various research domains, particularly within the sorption realm. Molecular metal oxide clusters, owing to their precisely tunable atomic structures and long-range order, exhibit significant potential as versatile platforms for sorption investigations. This study presents a series of isostructural Ti<sub>8</sub>Ce<sub>2</sub>-oxo clusters with subtle variations in coordinated linkers and explores their gas sorption behavior. Notably, Ti<sub>8</sub>Ce<sub>2</sub>-BA (where BA denotes benzoic acid) manifests a distinctive twostep profile during CO<sub>2</sub> adsorption, accompanied by a hysteresis loop. This observation marks a pioneering instance within the metal oxide cluster field. Of particular intrigue, the presence of unsaturated Ce(IV) sites was found to be correlated with the stepped sorption property. Moreover, the introduction of an electrophilic fluorine atom, positioned ortho or para to the benzoic acid, facilitated precise control over gate pressure and stepped sorption quantities. Advanced in-situ techniques systematically unraveled the underlying mechanism behind this unique sorption behavior. The findings elucidate that robust Lewis base-acid interactions are established between CO<sub>2</sub> molecules and Ce ions, consequently altering the conformation of coordinated linkers. Conversely, the F atoms primarily contribute to gate pressure variation by influencing the Lewis acidity of the Ce sites. This research advances the understanding in fabricating geometrically "flexible" metal-oxo clusters and provides profound insights into their host-guest interaction motifs. These insights hold substantial promise across diverse fields, particularly in CO2 gas capture and gas-phase catalysis, and offer valuable guidance for future adsorbent designs grounded in fundamental theories of structure-property relationships.

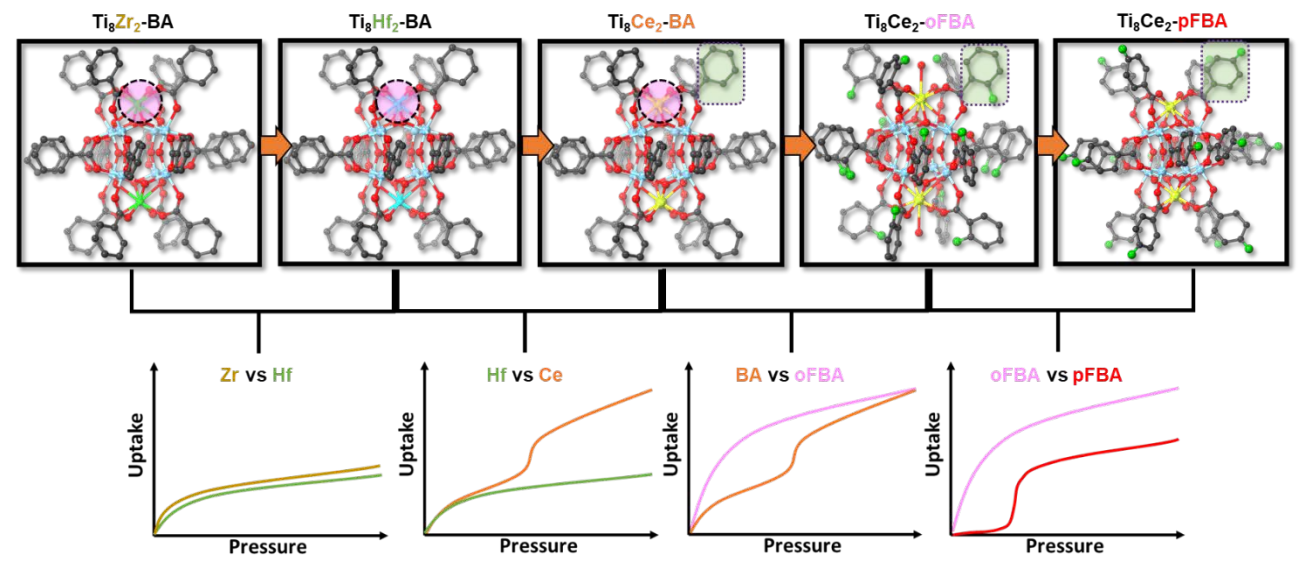
### **INTRODUCTION**

Normally regarded as geometrically rigid materials, metal oxide clusters are generally assembled by metal atoms and organic ligands that comprise bridging groups like carboxylic acids, hydroxyls, halides, and hydrides.<sup>1-4</sup> While their intrinsic properties with good stability and high reactivity make them useful in a range of industrial applications, their crystallographically well-defined structures with their high tunability have endowed them with great potential for being applied to fundamental studies in broad fields of chemistry, material science, and environmental science.<sup>5-10</sup> However, the limited porosity and surface area, compared to the extensively studied crystalline materials (like metal-organic frameworks (MOFs) or porous coordination polymers (PCPs), covalent organic frameworks (COFs), and hydrogen-bonded organic frameworks (HOFs)), have prevented researchers from deeply investigating their sorption properties. 10-15 So far, only a few papers have sought to study clusters' sorption performance, among which the majority typically only apply N<sub>2</sub> sorption isotherms under liquid nitrogen temperature to confirm their robust and permanently porous nature.<sup>3, 11, 16</sup> Beyond porosity studies, Zheng's group studied the CO<sub>2</sub> sorption and CO<sub>2</sub>/CH<sub>4</sub> separation performance with a series of high-nuclearity heterometallic Ni<sub>64</sub>Re<sub>96</sub> clusters, which present high selectivity of CO<sub>2</sub>/CH<sub>4</sub>.<sup>17</sup> In another work, Chun and colleagues reported several types of Ti-oxo clusters and investigated their CO<sub>2</sub> adsorption properties at 195 K; the results showed that while other clusters also present some  $CO_2$ uptake with nearly type-I isotherms.  $Ti_8O_{10}(abz)_{12}(PhCN)_{3.6}$  and  $Ti_6O_6(4-tbbz)_{10}(IPA)_2$  exhibit an additional subtle step in the adsorption profile that was attributed to the molecular packing expansion. 18, 19 Although these examples have been reported in the literature,

investigations of structure-property relationships and finetuning the sorption behaviors of metal oxide clusters remain unexplored. Metal oxide clusters, though less porous than MOFs and COFs, uniquely facilitate the study of guesthost interactions, particularly when single-crystal X-ray diffraction studies are performed. Metal oxide clusters serve as crucial sub-building blocks (SUBs) in the construction of MOFs. Nevertheless, directly investigating the guest-host interactions between these metal oxide clusters and guest molecules within MOFs, especially those characterized by relatively large porosity, poses challenges due to guest molecule disorder stemming from the framework's insufficient constraints. Therefore, metal oxide clusters with intrinsic porosity offer an excellent platform for exploring the fundamental nature of interactions between secondary building units (SBUs) and the specific guest molecules of interest with systematic tunings.

In this study, we selected Ti<sub>8</sub>Ce<sub>2</sub>-oxo clusters to explore the interactions between metal clusters and guest molecules. This choice was motivated by the inherent porosity observed in Ti<sub>8</sub>M<sub>2</sub> clusters in their solid-state form, as well as their established use as SBUs in MOF synthesis. where they have demonstrated intriguing properties.<sup>20</sup> By delving into how Ti<sub>8</sub>Ce<sub>2</sub> clusters interact with guest molecules, we aim to gain valuable insights into how these clusters will engage with guest molecules within MOFs. Remarkably, the Ti<sub>8</sub>Ce<sub>2</sub> cluster exhibited a markedly distinct sorption behavior with CO2, hinting at a complex and nontrivial interplay between the guest and host interactions emanating from the metal center. The introduction of a fluorine substituent on the benzoate group offers valuable insights into the subtle means by which we can precisely tailor the interactions between the metal cluster and guest CO<sub>2</sub> molecules at an atomic scale (Scheme 1). Examining

Scheme 1. Cluster structure illustration in this work and its key element variation in regulating the flexibility property.



Minor Variations in Structure Make Huge Difference toward "Flexible" Sorption Performance

the subtle size differences between fluorine and hydrogen substituents (1.47 Å vs 1.20 Å),<sup>21-24</sup> the impact of fluorine substitutions primarily influences the electron-donating capacity of the coordinating carboxylate groups, rather than exerting a significant steric effect. This capability allows us to finely tune the Lewis acidity of the metal sites directly involved in interactions with guest-host molecules. A series of in-situ techniques, including in-situ single crystal X-ray diffraction (SCXRD), in-situ powder X-ray diffraction (PXRD), and in-situ CO<sub>2</sub> sorption isotherms and infrared spectroscopy (IR), were applied to deeply investigate the underlying mechanisms. These results reveal that both Ce and F contribute to the stepwise sorption phenomenon but in different manners, which can provide researchers with intuitive information to further understand the interactions between gas molecules and the porous cluster lattice, paving the way for the future design of tailored adsorbents with diverse functionalities.

### RESULTS AND DISCUSSION

The synthesis of  $Ti_8Ce_2$ -BA followed our previously reported procedure. To be noted, the cluster is capped by 16 benzoate ligands, with the two Ce sites being eight-coordinated in a square antiprismatic geometry and all eight Ti sites being six-coordination in an octahedral coordination geometry. The discrete clusters are densely packed in a highly-ordered manner with the presence of  $\pi$ - $\pi$  stacking interactions between the staggered ligands, resulting in the

generation of a one-dimensional pore (lattice voids formed by surrounding benzene rings) in the a direction (**Figure 1a**).

The cluster was then subjected to a gas sorption performance study. Negligible uptake was observed for both N<sub>2</sub> at 77 K (Figure S1a) and Ar at 87 K (Figure S1b). However, a significant quantity of CO<sub>2</sub> molecules reaching approximately 70 cm<sup>3</sup>/g was adsorbed at 195 K under 1 bar (Figure 1b). Interestingly, the isotherm exhibited a distinct secondary sorption step at a pressure of around 0.4 bar. This sorption step was reversible with a H1-type hysteresis loop; a phenomenon that has been previously reported for flexible MOFs,<sup>26-29</sup> COFs,<sup>30, 31</sup> and HOFs;<sup>32-34</sup> but, to the best of our knowledge, is the first to be discovered in the metal oxide cluster domain. The sorption behavior was then primarily investigated by measuring other gas isotherms, including NH<sub>3</sub>, CO, C<sub>2</sub>H<sub>2</sub>, and O<sub>2</sub>, and the results showed that NH<sub>3</sub> adsorption isotherm also presented a stepped sorption from 0.1 to 0.2 bar at 273 K (Figure 1c). In contrast, other tested gases presented no sorption steps (Figures S1c, d and S2a, b), suggesting that the occurrence of the phenomenon might be related to the physical properties of the adsorbate. It's also worth noting that the only gases exhibiting sorption steps are CO2 and NH3 which can act as Lewis bases at their O and N sites, respectively, while the other gases cannot. Indeed, this was later confirmed to be the main

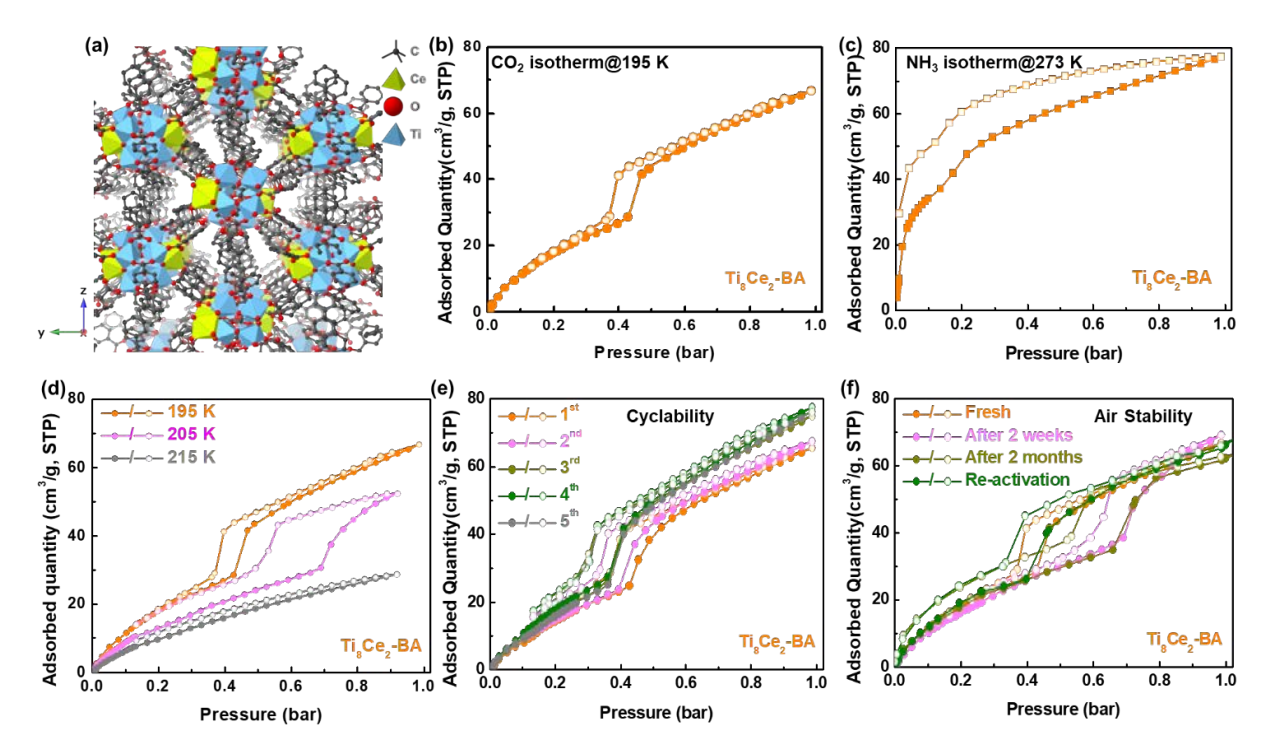


**Figure 1.** Structure and sorption performance of Ti<sub>8</sub>Ce<sub>2</sub>-BA. a) Packed structure with one-dimension pore; b) CO<sub>2</sub> isotherm at 195 K; b) NH<sub>3</sub> isotherm at 273 K; d) CO<sub>2</sub> isotherms at varied temperatures; e) cyclability test for CO<sub>2</sub> sorption at 195 K; f) air stability test.

cause contributing to the occurrence of the stepped sorption isotherms for these gases (*vide infra*).

We then further explored the stepped sorption behavior with variable-temperature  $CO_2$  isotherms. **Figure 1d** shows that the gate pressure shifted to higher pressure of  $\sim 0.7$  bar with a lower total  $CO_2$  uptake when the test temperature rose to 205 K, and the stepped sorption disappeared when measured at 215 K with a further decreasing  $CO_2$  sorption capacity, indicating its physical sorption nature. From the data collected at three different temperatures, we observed that the secondary sorption step shifts to the higher-pressure range as the temperature increases, and it moves beyond our measured pressure range (1 bar) when the temperature exceeds 215 K.

To test our hypothesis, we selected water, which can also act as a Lewis base with the oxygen atom, as another analyte. The water sorption isotherm collected at 298 K shows a stepped increase starting from 60% relative humidity (RH) that still does not saturating at 90% RH (**Figure S2d**). The overlapping of isotherms from three consecutive cycles demonstrated that the cluster's structure can be maintained even under strong capillary forces. Next, the cluster's cyclability underwent analysis (**Figure 1e**), revealing a nearly consistent sorption behavior. However, a subtle shift

in gate pressure towards the lower range and an increased total uptake were observed. These alterations could potentially be attributed to the gradual relaxation of the crystal lattice after multiple activations, leading to an augmented affinity of the pore environment for the adsorbate. Lastly, we examined the air stability of the cluster. As shown in Figure 1f, even after 2 weeks and 2 months of exposure to air, the cluster exhibited similar uptake of CO<sub>2</sub> relative to that of the freshly prepared sample, but showed a large shift of the gate-pressure to higher pressures. We postulate that this shift may be due to the presence of some molecules with strong adhesion to the surface/binding sites that still reside in the lattice void after the first activation (See SI for more detailed discussion). Nevertheless, the clusters revert to their original CO<sub>2</sub> sorption profile right after the second activation, demonstrating their air stability.

To gain insights into the structural aspect that results in these uncommon sorption phenomena, we synthesized two isostructural clusters, namely  $Ti_8Zr_2$ -BA and  $Ti_8Hf_2$ -BA, and used them as points of comparison in our  $CO_2$  sorption study. While the identical structural conformation was validated by the SCXRD data (**Table S1**), systematical characterizations also proved the successful synthesis of the clusters (**Figures 2a** and **S5-S7**).  $CO_2$  isotherms were then

collected for these clusters (Figures 2b and S8), which show that both the Zr and Hf analogues exhibited no stepped sorption profiles and relatively lower total uptakes of CO<sub>2</sub> of ~24 cm<sup>3</sup>/g, suggesting that this unique sorption behavior might have a high relevance to the Ce species. In the typical scenarios, Zr and Hf metal sites exhibit an inherent 8-coordinate configuration. In contrast, despite being the least Lewis acidic in the hexametric clusters,35 Ce centers show a unique propensity for transitioning to higher coordination states, notably as 9-coordinated entities. This distinction is significant: whereas Zr and Hf, when fully capped with carboxylate groups, become coordination saturated, Ce has the potential for additional interactions. This capability allows Ce to engage in extra interactions, specifically with guest CO<sub>2</sub> molecules. Indeed, the crucial role of Ce(IV) sites as Lewis acid sites, pivotal in enabling their interaction with guest CO2 molecules, has been underscored in the literature.35,36

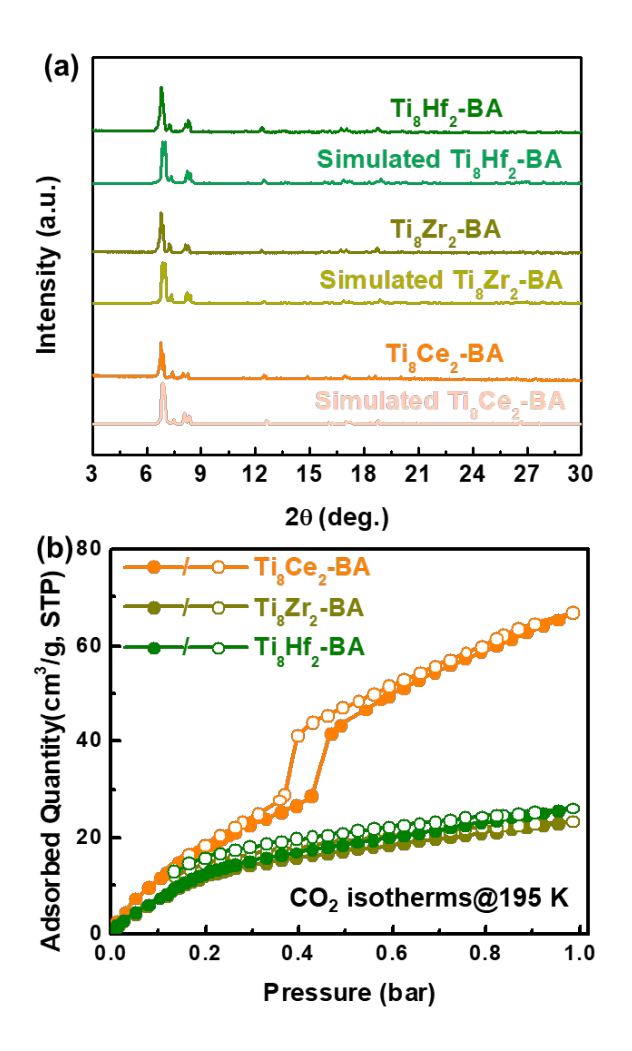


**Figure 2.** Structure and sorption performance comparison among  $Ti_8M_2$ -BA (M=Zr, Hf, Ce). a) Experimental and simulated PXRD patterns; b)  $CO_2$  isotherms at 195 K.

Building upon our earlier hypothesis, the interactions between Ce sites and CO2 guest molecules are intricately linked to the Lewis acidity of the Ce sites. The precise modulation of these Ce-CO<sub>2</sub> interactions is achieved through the partial or complete substitution of the BA ligand with its fluorinated derivatives. Given the similarity in Van der Waals radii between fluorine and hydrogen, the steric effect of fluorine substitutions becomes negligible. This yields the successful synthesis of isostructural analogs, Ti<sub>8</sub>Ce<sub>2</sub>-oFBA and Ti<sub>8</sub>Ce<sub>2</sub>-BA/pFBA, accomplished through similar synthetic procedures, except for the ful and/or partial replacement of benzoic acid with ortho-fluorobenzoic acid (oFBA) and para-fluorobenzoic acid (pFBA), respectively. The structures of these clusters were confirmed by both SCXRD and PXRD analysis (Figures 3a, d and Figures 4a, c). Therefore, the Lewis acidity of the Ce sites primarily hinges on the electron-donating capacity of the coordinating carboxylate groups, a trait often correlated with their respective pKa values. Considering the descending trend in pKa values from BA to pFBA and oFBA (4.20, 4.14, and 3.27 respectively),<sup>37</sup> one anticipates a corresponding rise in the Lewis acidity of the Ce sites from BA to pFBA, with oFBA presumed to exhibit the highest Lewis acidity and subsequently the strongest interaction with guest CO<sub>2</sub> molecules among this series.

Firstly, the Ti<sub>8</sub>Ce<sub>2</sub>-oFBA case was examined through SCXRD analysis (Figure 3a). While a similar packing pattern to that of Ti<sub>8</sub>Ce<sub>2</sub>-BA was present, we observed a coordination variation in the Ce site. In contrast to the 8coordinate environment of the Ce sites in the Ti<sub>8</sub>Ce<sub>2</sub>-BA case, the Ti<sub>8</sub>Ce<sub>2</sub>-oFBA version exhibits a quasi-9-coordinate structure. This variant presents an additional weakly coordinating water molecule, fostering a relatively long Ceoxygen bond (2.724 Å) directed toward a lattice void (Figure 3b) and stabilized with hydrogen bonds between the water molecule and fluorine (HO-H···F, Do-F=3.375 Å, **Figure 3c**). Interestingly, despite the formation of hydrogen bonds combined with the steric effects from the benzoate, no crystallographic disorder of F atom was found in the structure. The presence of an additional coordinated water implies heightened accessibility to the Ce site, attributed to the increased Lewis acidity. Upon activation under vacuum at 120 °C, it's believed that the weakly coordinating water molecules on the Ce sites are removed, leaving the coordination sites open for interactions with CO<sub>2</sub> molecules (implied by the peak shifts of the VT-PXRD (**Figure S9b**)). This hypothesis aligns with its rapid initial uptake of  $CO_2$  at low pressure (< 0.1 bar) and nearly equivalent uptake at higher pressure (> 0.4 bar) compared to the  $Ti_8Ce_2$ -BA version (**Figure 3e**). A similar consequence is also observed

in the case of  $NH_3$  adsorption at 273 K, where a higher  $NH_3$  sorption affinity at low pressure compared to that of  $Ti_8Ce_2$ -BA and the absence of a stepped sorption was presented (**Figure 3f**).

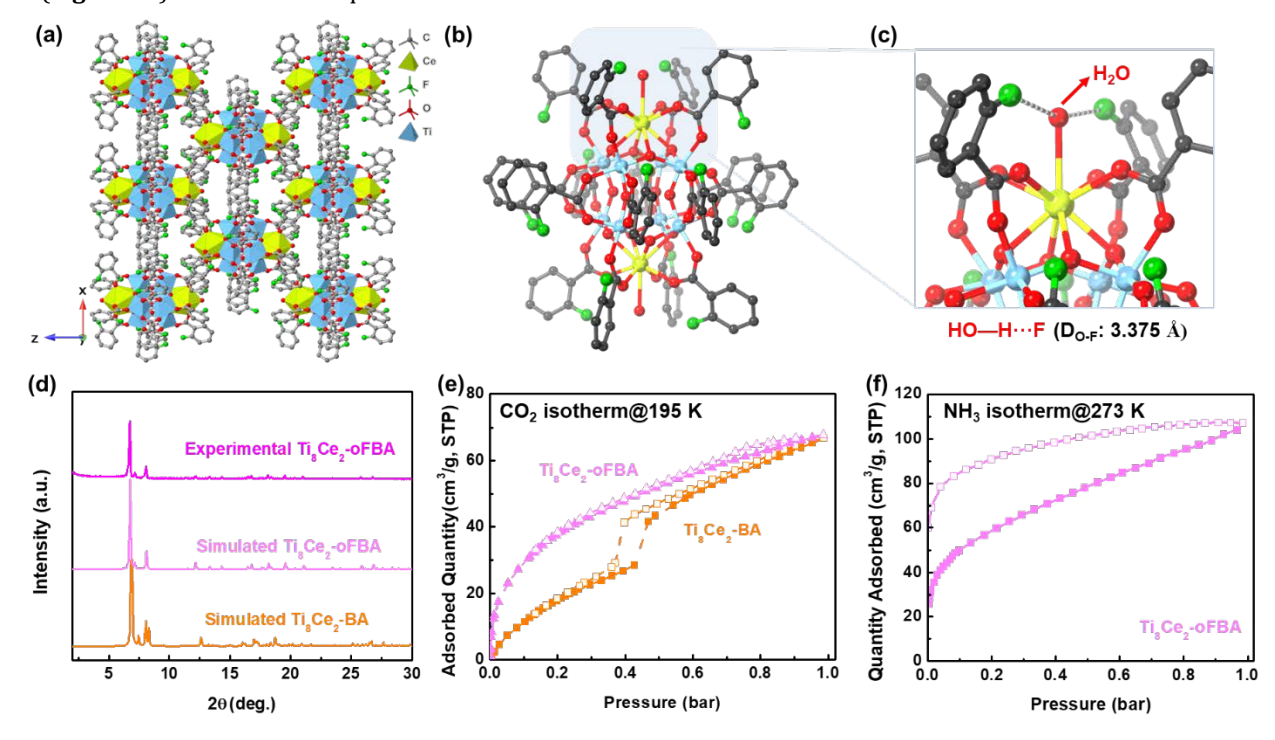


**Figure 3.** Structure and sorption performance of Ti<sub>8</sub>Ce<sub>2</sub>-oFBA. a) Packed structure with one-dimension pore; b) Structure of single cluster; c) Detailed local binding environment of Ce on single cluster; d) Experimental and simulated PXRD patterns; e) CO<sub>2</sub> isotherms at 195 K; f) NH<sub>3</sub> isotherm at 273 K.

To expand upon the isolated cases of Ti<sub>8</sub>Ce<sub>2</sub>-BA and Ti<sub>8</sub>Ce<sub>2</sub>-oFBA, a spectrum was explored by partially substituting BA with oFBA at levels of approximately 10, 20, 30, 50, and 75%, which were confirmed by PXRD analysis (Figures 4a and S10), proton nuclear magnetic resonance spectroscopy (1H NMR, Figure S11), scanning electron microscopy (SEM, Figure S12), and IR spectroscopy (Figure S13). Noted, the ratios shown on the sample labels are the percentages of the linkers that being added to the synthesis solution, which were later found to be comparable to the real coordinated ratios on the clusters (Figure S11f). For example, 80% BA/20% oFBA represented the cluster that was synthesized by using 2.4 mmol BA and 0.6 mmol oFBA (total 3 mmol), while its final BA:oFBA ratio on the cluster is 78%:22% (Figure S11b). The CO2 sorption isotherms at 195 K were measured for the modulated samples and are depicted in Figure 4b for comparison. As the percentage of oFBA substitution increases, a consistent shift of the pressure of the step towards the low-pressure region (from 0.35 to 0.05 bar) is observed. When the

substitution rates of oFBA surpass 50%, convergence occurs rapidly towards that of the Ti<sub>8</sub>Ce<sub>2</sub>-oFBA sample (Figure S14). This phenomenon can be explained by the increased substitution rates of BA with oFBA, enhancing the Lewis acidity of the Ce sites and thereby intensifying their affinity for CO<sub>2</sub> molecules. Consequently, this leads to the shift of the gate opening pressure towards the low-pressure region (Figures 4b and S14f). The near-convergence observed in samples above substitution rates of oFBA above 50% suggests that the Lewis acidity of the Ce sites is opening sufficiently elevated to facilitate accommodating coordination from the additional guest molecule. Control experiments performed with physical mixtures of single-linker clusters (Table S5) demonstrate that the sorption properties described above originate from the behavior of the mixed-linker clusters rather than from physical mixtures of two single-linker clusters (Figures 4c, 4d, and S15-17).

With the weakly coordinating water on the Ce sites serving as a potential indicator of their Lewis acidity, SCXRD

measurements were conducted to uncover structure-property relationships, thereby solidifying our conclusions on correlation between Lewis acidity and  $CO_2$  sorption behavior. Two clusters were chosen for the study, including  $Ti_8Ce_2$ -80% BA/20% oFBA and  $Ti_8Ce_2$ -65% BA/35% oFBA. Similar structures were found besides the occupancy of

weakly coordinating water molecules. For the  $Ti_8Ce_2-80\%$  BA/20% oFBA sample (**Figures 4e** and **S14(b)**), corresponding to a 0.12 bar gate opening pressure, the lower Lewis acidity due to the lower oFBA substitution rate resulted in a crystallographic

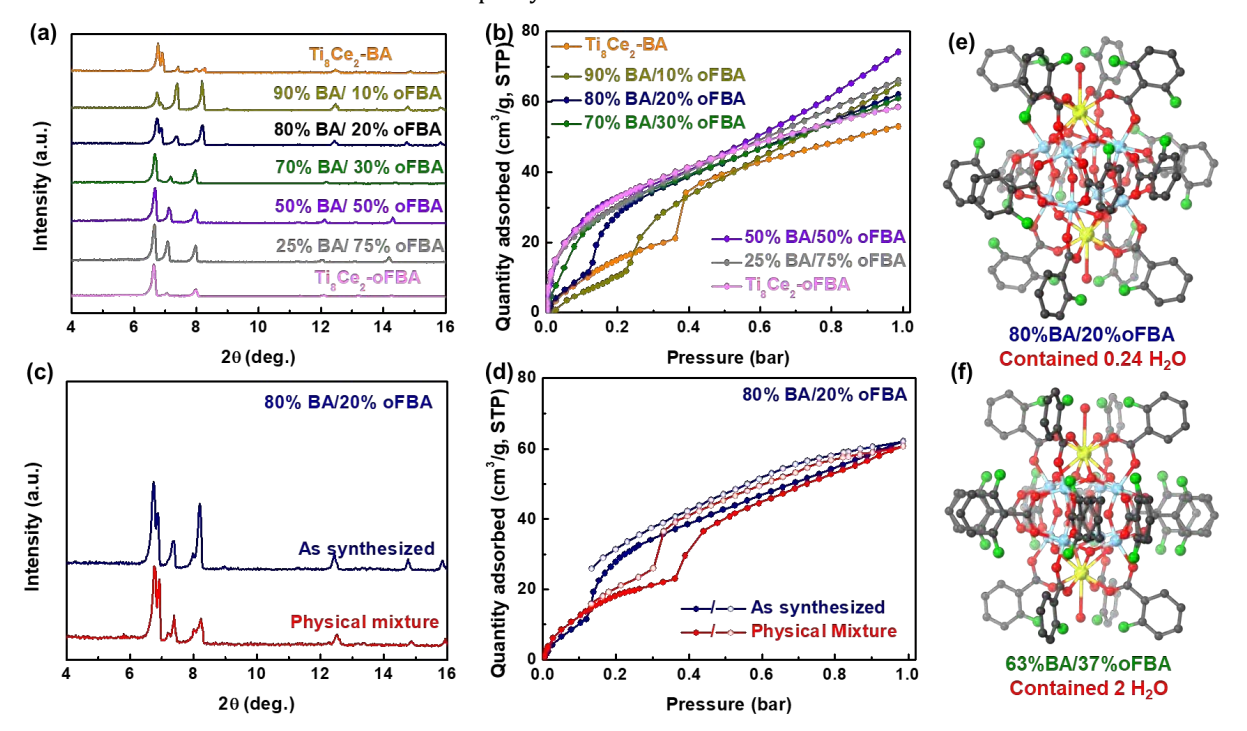


**Figure 4.** Structure and sorption performance of  $Ti_8Ce_2$ -BA/oFBA. a) Experimental PXRD patterns for mix-linker clusters with various ratios; b)  $CO_2$  isotherms at 195 K; c) PXRD pattern comparison between as synthesized and physical mixture samples; d)  $CO_2$  sorption performance comparison; e) Structure of single cluster for  $Ti_8Ce_2$ -80% BA/20% oFBA; f) Structure of single cluster for  $Ti_8Ce_2$ -65% BA/35% oFBA.

occupancy of 0.24  $H_2O$  per cluster. Regarding the  $Ti_8Ce_2-65\%$  BA/35% oFBA sample (**Figures 4f** and **S18**), associated with a gate opening pressure lower than 0.1 bar, the refined occupancy of water molecules reached 2  $H_2O$  per cluster. This suggests that the Ce sites exhibit sufficient Lewis acidity to accommodate one full water molecule per site with 35% oFBA substitution rate. Moreover, the correlation observed between water occupancies and the gate opening pressure in the  $CO_2$  isotherms reinforces the assertion that the interaction between Ce and  $CO_2$  can be finely modulated by altering the Lewis acidity of the Ce sites. This adjustment is achieved through changes in the electron-donating properties of the capping ligands.

To eliminate the potential influence of the steric effects caused by the adjacent fluorine atoms within the coordinating sphere, and to confirm that the pKa of the benzoate group, which is directly linked to the Lewis acidity of the Ce center, is the primary determining factor, the para-

fluorobenzoic acid (pFBA) ligand was selected due to its lower pKa (4.14) compared to the benzoic acid (4.20) but without potential steric effects around the Ce sites. PXRD analysis (Figure 5a) and other characterization results (Figures S19-21) confirmed the successful synthesis of Ti<sub>8</sub>Ce<sub>2</sub>-BA/pFBA with varied linker ratios. Moreover, SCXRD analysis verified the absence of H<sub>2</sub>O molecules on the Ce sites for clusters with two different BA/pFBA ratios (Figures 5b and 5c), which suggests a moderate Lewis acidity of the Ce sites in these clusters. Gas sorption studies were then carried out, and Figures 5d-f show the CO2 isotherms of Ti<sub>8</sub>Ce<sub>2</sub>-BA/pFBA under 195 K with varied BA/pFBA ratios. Interestingly, a sharp and much more distinguished step in the sorption isotherm was observed, as well as a similar gate-pressure shifting phenomenon, with increasing pFBA introduction. When 5% pFBA was introduced, the stepped sorption occurred around 0.3 bar, and it decreased to the pressures of 0.25 and 0.12 when 10% and 20% pFBA were introduced, respectively. This interesting and unique sorption property observed on the cluster was ascribed to enhancement of the Lewis acidity of the Ce sites. To further support this proposed hypothesis, isostructural  $Ti_8Zr_2$ -90% BA/10% pFBA (**Figure S22a**) and a  $Ti_8Ce_2$ -98% BA/2% pFBA (**Figure S23a**) were synthesized and applied for the  $CO_2$  isotherms at 195 K. While no stepped sorption was observed for  $Ti_8Zr_2$ -90% BA/10% pFBA (**Figure S22b**, **Table S3**), an intermediate stepped

sorption behavior between  $Ti_8Ce_2$ -BA and  $Ti_8Ce_2$ -95% BA/5% pFBA was found on  $Ti_8Ce_2$ -98% BA/2% pFBA (**Figure S23b**). These findings reaffirm that the gate opening effect of the  $CO_2$  adsorption isotherm is attributed to the accessible Lewis acidity of the Ce sites within the  $Ti_8Ce_2$  cluster.

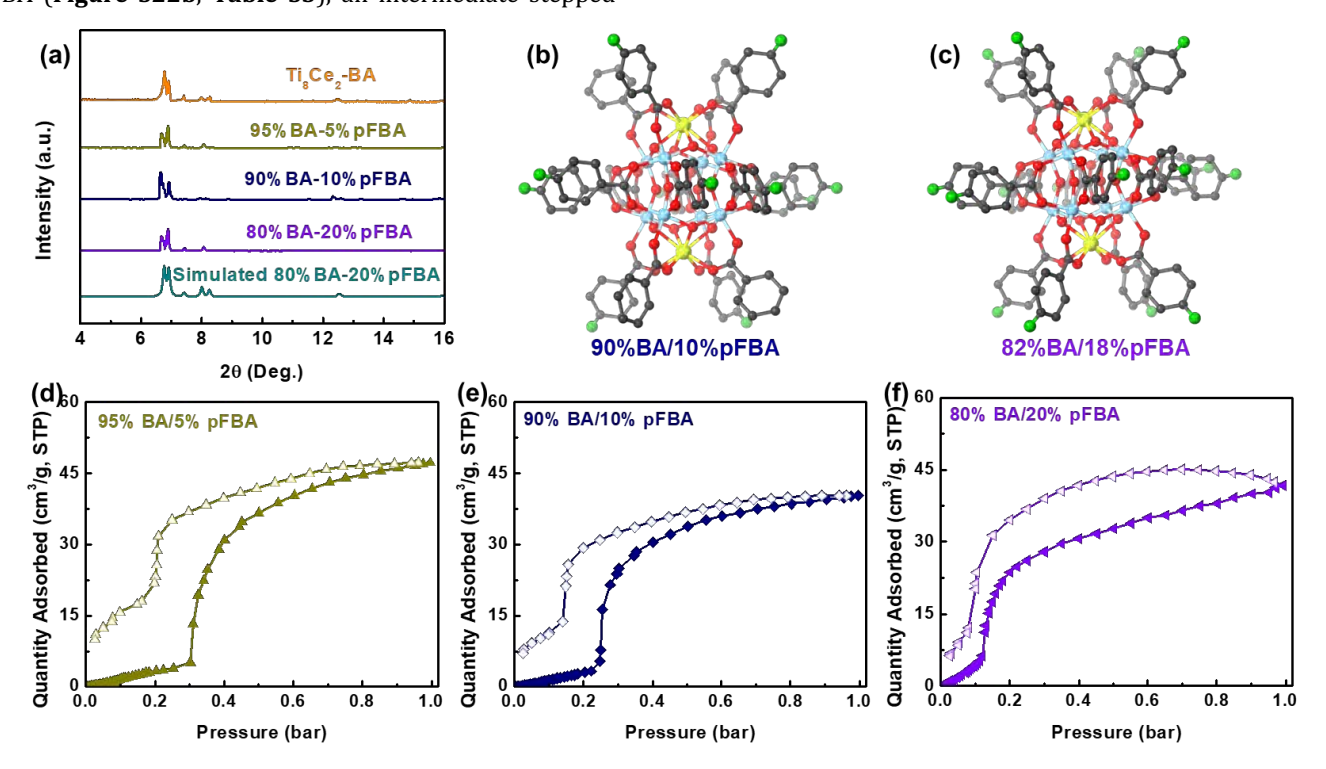


**Figure 5.** Structure and sorption performance of  $Ti_8Ce_2$ -BA/pFBA. a) Experimental PXRD patterns for mix-linker clusters with various ratios; b) Structure of single cluster for  $Ti_8Ce_2$ -90% BA/10% oFBA; c) Structure of single cluster for  $Ti_8Ce_2$ -82 %BA/18% oFBA; CO<sub>2</sub> isotherms measured at 195 K for d)  $Ti_8Ce_2$ -95% BA/5% oFBA, e)  $Ti_8Ce_2$ -90% BA/10% oFBA, and f)  $Ti_8Ce_2$ -80% BA/20% oFBA.

Moreover, these results highlight the high adjustability of this effect through deliberate designs involving the capping benzoate group, directly influencing the Lewis acidity of the Ce sites. The stepped sorption, though not as obvious, was also observed in the NH $_3$  adsorption isotherms (**Figure S24**). Furthermore, cycled CO $_2$  sorption tests carried out on Ti $_8$ Ce $_2$ -95% BA/5% pFBA and Ti $_8$ Ce $_2$ -90% BA/10% pFBA (**Figure S25**) showed similar relaxation behavior between cycles, confirming that their structures are well retained during the CO $_2$  sorption tests.

To study the structural flexibility on the clusters, in-situ PXRD studies were carried out. Control experiments were also carried out and showed as **Figure S26**. When the PXRD data was collected at lower temperatures, diffraction peaks

shifted to higher angles, indicating the unit cell (lattice parameters) could be affected by temperature and shrink at lower temperatures. On the other hand, subjecting the samples to vacuum at room temperature (RT) and subsequently filling the sample with CO<sub>2</sub> does not result in a change in the peak positions. Based on these results, systematic studies were then conducted on Ti<sub>8</sub>Ce<sub>2</sub>-BA (**Figure S28a, S28b**), Ti<sub>8</sub>Hf<sub>2</sub>-BA (**Figure S28c, S28d**), and Ti<sub>8</sub>Ce<sub>2</sub>-90% BA/10% pFBA (**Figure S29**) through adjusting the test conditions. The results show that only Ti<sub>8</sub>Ce<sub>2</sub>-BA and Ti<sub>8</sub>Ce<sub>2</sub>-90% BA/10% pFBA present an expansion to a higher lattice parameter when they are filled with CO<sub>2</sub> under 1 bar at 195 K (**Table S6** and **S8**), and they return to their original state with the

application of vacuum, confirming their "flexible" nature and being consistent with the observed sorption behaviors. In contrast, but as expected,  $Ti_8Zr_2$ -BA and  $Ti_8Hf_2$ -BA do not show any changes before and after the  $CO_2$  adsorption (**Table S7**). Based on the in situ PXRD results, our conclusion leans towards structural alterations in the solid state being primarily attributed to changes in the coordination number of Ce Lewis acid sites, a phenomenon not observed in the Zr and Hf variants.

Given all this indirect proof presented, we then attempted to observe interactions between the adsorbate and the adsorbent with atomic precision through SCXRD analysis to obtain an insightful understanding on the structure-property relationship. In-situ SCXRD with  $CO_2$  adsorption was then carried out by accurately controlling the pressure, according to the position of the step of the  $CO_2$  isotherm collected at 195 K, to obtain different states of the structure (see SI for more experimental details).

Figure 6a shows the packed structure of Ti<sub>8</sub>Ce<sub>2</sub>-BA from the a direction under vacuum at 196 K (See SI for more experimental details). As CO2 filled into the sample, the pressure was carefully controlled to be lower than 0.4 bar, at which point the cluster was allowed to equilibrate for 2 hours, resulting in only the first sorption stage. The SCXRD data was then collected, and the resulting structure is shown as **Figure 6b** and **4e**, which presented some electron clouds inside the lattice voids. Though we postulate these clouds to be CO<sub>2</sub> molecules, the disordered nature rendered them unable to be refined crystallographically. This phenomenon arises due to the physisorption nature characterized by weak interactions between the adsorbate (CO<sub>2</sub> molecules) and adsorbent (the cavity), resulting in a lack of long-range ordering in the arrangement of CO2 molecules (Figure 6e). Consequently, this arrangement cannot be effectively probed using SCXRD analysis. As we increase the pressure further to around 1 bar, where the

stepped sorption has occurred, the structure clearly showed  $CO_2$  molecules inside the voids and the adsorbed  $CO_2$  was found with no disorder and with 100% occupancy (**Figure 6c**). A close inspection shows that a  $CO_2$  molecule sits closely to the unsaturated Ce site with a Ce-O distance of 3.401 Å at 1 bar (**Figure 6f**), directly showcasing the presence of a strong interaction between the  $CO_2$  and the Ce site, as this distance is significantly shorter than the sum of the van der Waals radii of cerium (2.48 Å) and oxygen (1.52 Å). This strong interaction results from the Lewis acid-base interaction.

Structural conformation changes of the cluster before and after CO2 adsorption were also investigated to further correlate structural changes with the sorption behavior. As shown in Figure 6g, the preliminary angle of 01 (from carboxylate group of BA1)-Ce-O2 (from carboxylate group of BA2) is around 122.11°, while the dihedral angle for the other two capping BA linker is 0°. As the pressure increases to 1 bar and CO2 binds to the Ce sites, we notice that the angle for O1-Ce-O2 expands to 123.4° and the dihedral angle for the parallel BAs increases to 12.6° due to the rotation of coordinated linkers. Moreover, the unit cell of Ti<sub>8</sub>Ce<sub>2</sub>-BA displays a slight expansion in all dimensions post CO<sub>2</sub> adsorption (**Table S9**). These variations in the microscopic structure of Ti<sub>8</sub>Ce<sub>2</sub>-BA were then attributed to the strong interactions between the CO2 molecules and the Ce sites, which induce a quasi-chemisorption of CO<sub>2</sub> molecules to the coordination sphere of Ce, resulting in the occurrence of stepped sorption. Based on our analysis, we propose that in Ti<sub>8</sub>Ce<sub>2</sub>-BA, CO<sub>2</sub> initially undergoes adsorption in lattice voids with disordered distributions. As the pressure rises, the increasing free energy of CO2 molecules can overcome the energy barrier necessary for modifying the configuration of the Ce coordination sphere, which involves variations in both the coordination

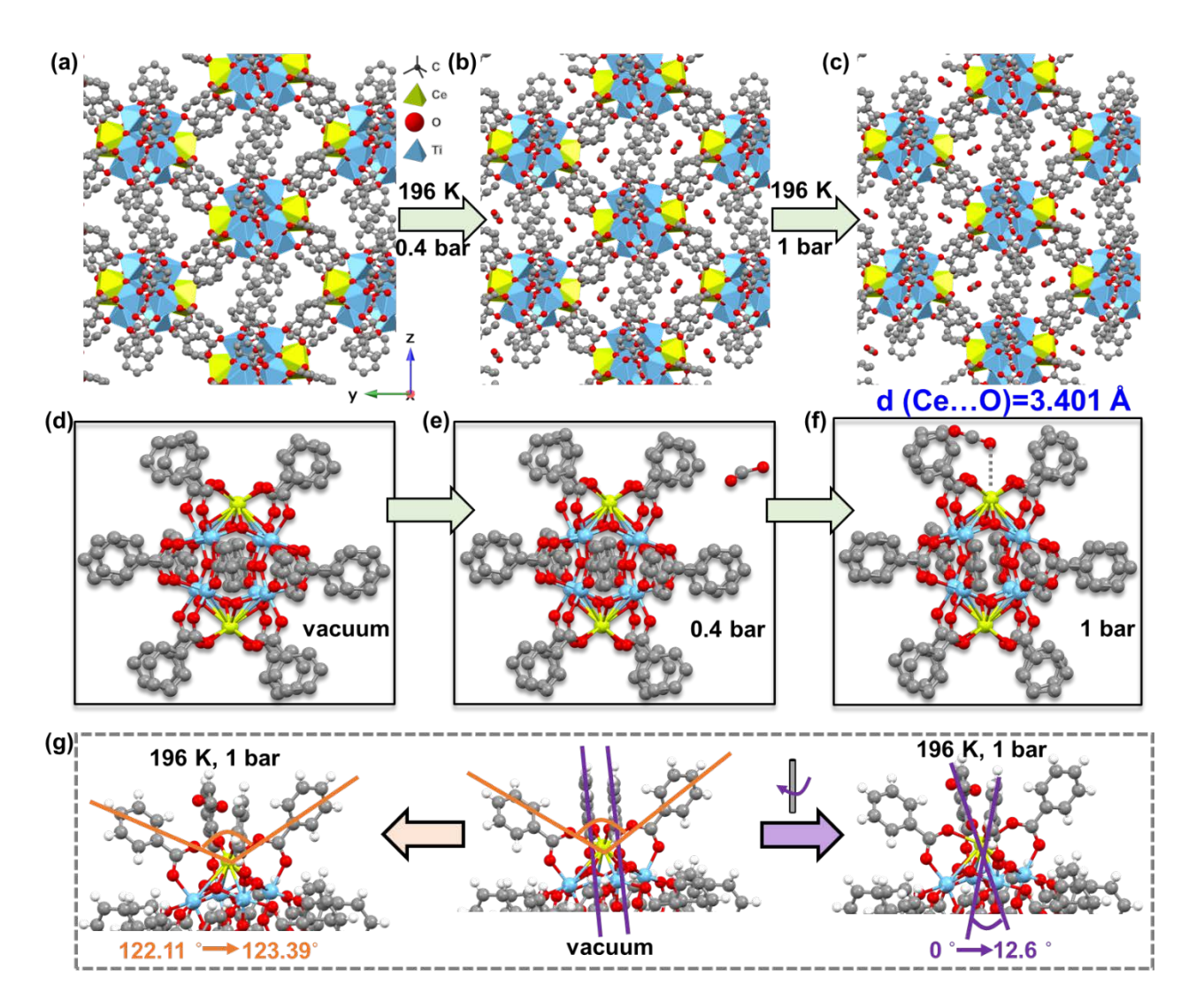


**Figure 6.** In-situ SCXRD measurements of  $CO_2$  sorption on  $Ti_8Ce_2$ -BA. a, d) Crystal structures of packed cluster and single cluster under vacuum condition; b, e) Crystal structures of packed and single cluster under 0.4 bar  $CO_2$ . Noted, the  $CO_2$  molecule was assigned to show the potential position of the  $CO_2$  molecules based on the Q peaks and not actually refined; c, f) Crystal structures of packed cluster and single cluster under 1 bar  $CO_2$ ; g) Structure conformation change under 1 bar  $CO_2$  at 196 K.

number and geometric structure. This alteration leads to the formation of Ce-O (O from O=C=O) interactions, ultimately resulting in a notable gate-opening effect. The detailed  $CO_2$  distribution inside the lattice voids at different stages is also discussed (see SI for more information).

The same protocol was then applied to the  $Ti_8Ce_2-90\%$  BA/10% pFBA for the  $CO_2$  sorption study, as shown in **Figure 7**. Likewise, the structural observation (**Figures 7b** and **7e**) revealed an absence of  $CO_2$  molecules when exposed to 0.2 bar  $CO_2$  for equilibration of 2 hours. This absence stems from the inherent lack of long-range ordering characteristic of physisorption at this specific pressure (**Figure 5e**). Further investigation of the crystal structure revealed the additional reason for the almost negligible  $CO_2$ 

uptake at the low-pressure region. The void space of the  $Ti_8Ce_2$ -90% BA/10% pFBA was calculated and compared to that of  $Ti_8Ce_2$ -BA (**Figure S30**). As expected, the size of the lattice void is smaller for  $Ti_8Ce_2$ -90% BA/10% pFBA than that for  $Ti_8Ce_2$ -BA, which could hinder the access of  $CO_2$  into the voids to some extent and is consistent with the lower  $CO_2$  uptake at the initial adsorbed state compared to  $Ti_8Ce_2$ -BA. The smaller void space (7.9% for  $Ti_8Ce_2$ -BA and only 6.6% for  $Ti_8Ce_2$ -90% BA/10% pFBA) also accounts for the decreasing total  $CO_2$  uptake (**Figures 5d-5f**). Interestingly, when the pressure increased to 1 bar, similar amount of  $CO_2$  molecules with the same interaction with the Ce site was observed where the distance of Ce-0 (0=Ce-0) is measured to be 3.417 Å, being almost equal to the value observed in

Ti<sub>8</sub>Ce<sub>2</sub>-BA (*vide supra*) (**Figure 7c** and **7f**). Moreover, structural analysis presented similar conformation changes

as well, with an angle expansion from  $121.9^{\circ}$  to  $123.2^{\circ}$  on the

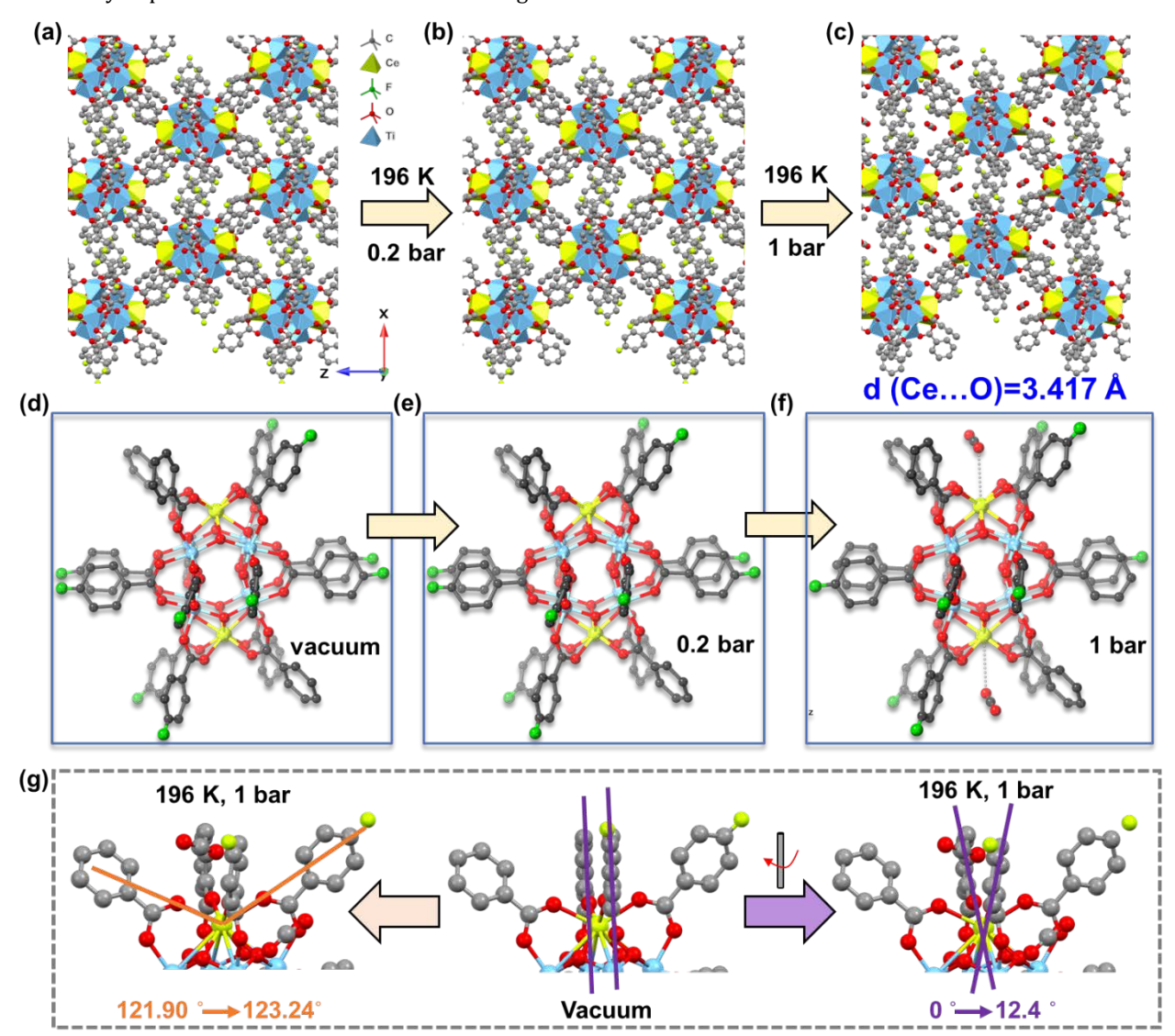


**Figure 7.** In-situ SCXRD measurement of  $CO_2$  sorption on  $Ti_8Ce_2$ -90% BA/10% pFBA. a, d) Crystal structures of packed cluster and single cluster under vacuum condition; b, e) Crystal structures of packed and single cluster under 0.2 bar  $CO_2$ ; c, f) Crystal structures of packed cluster and single cluster under 1 bar  $CO_2$ ; g) Structure conformation change under 1 bar  $CO_2$  at 196 K.

O1-Ce-O2 together with a 12.4° difference on the dihedral angle for the other two capping BA linkers (**Figure 7g**). More comparisons between  $Ti_8Ce_2$ -BA and  $Ti_8Ce_2$ -90% BA/10% pFBA on the lattice cell parameters and  $CO_2$ -filled structures can be found in **Tables S9** and **S10**. With the findings above, the adsorption mechanism in the case of  $Ti_8Ce_2$ -90% BA/10% pFBA is then believed to be similar to what we have claimed for the  $Ti_8Ce_2$ -BA but with some differences: the  $CO_2$  was excluded outside the cluster at the very beginning due to the narrower "pore aperture", and the strong interaction between  $CO_2$  and Ce site acts as the "key" to force the "gate" (bond angle expansion and linker rotation) open and enables the entrance of  $CO_2$  molecules. Thus, it is

proposed that the stepped sorption would occur once the "gate" opens. With the findings derived from in-situ SCXRD analysis, we've directly highlighted the interaction between Ce and CO<sub>2</sub> through a Lewis acid-base coordination. This technique enabled the precise exploration of atomic-level interactions between the adsorbate and adsorbent, facilitating a comprehensive understanding of the actual mechanism behind the observed phenomena.

In addition to the structural insights into the  $Ce\text{-}CO_2$  interactions provided by SCXRD analysis, in-situ  $CO_2$  adsorption-IR measurements offer a means to investigate electronic-level interactions. This method allows us to discern the intensity of interactions by analyzing the

vibration frequencies of the chemical bonds, providing valuable information regarding the strength and nature of these interactions. The in-situ IR spectra were collected at selected data points on isotherm curves and subtracted by the IR spectra of corresponding clusters (**Figure** 

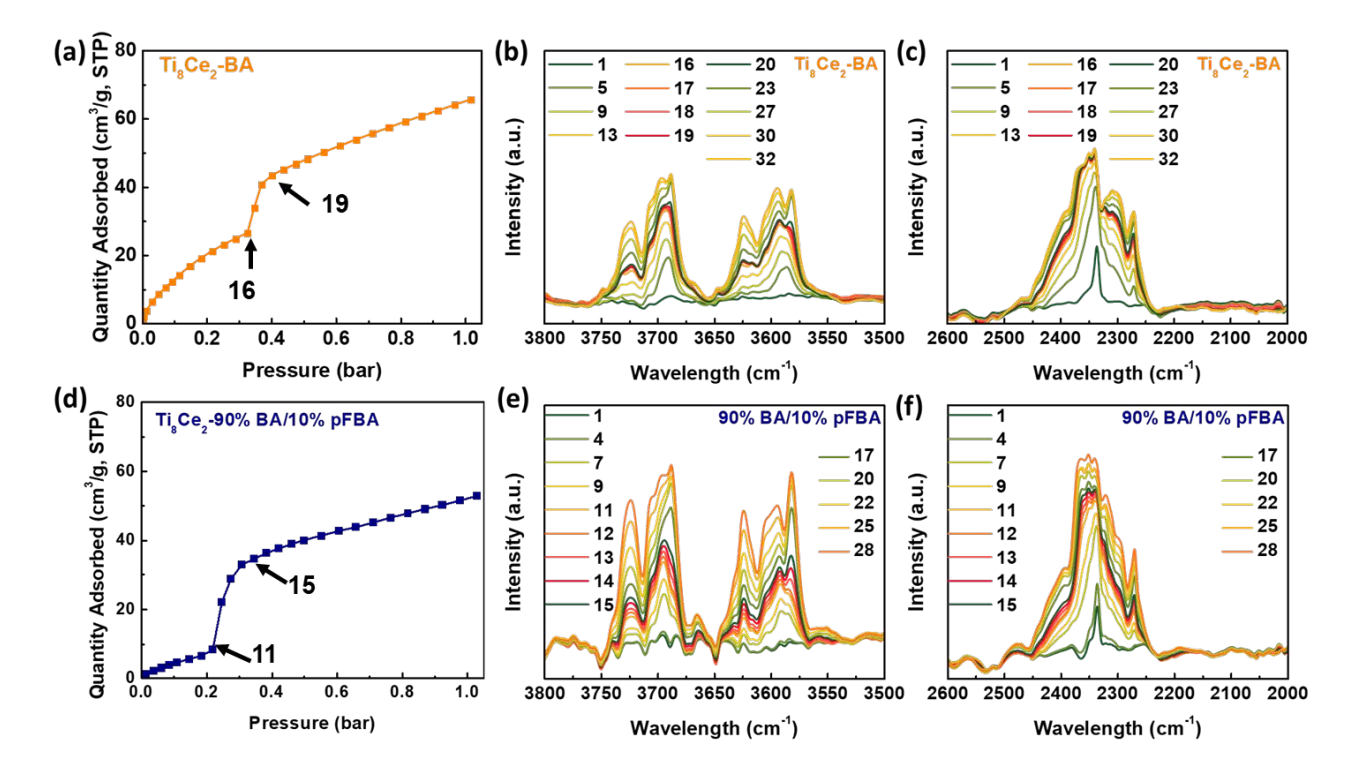


**Figure 8.** In-situ IR measurement with  $CO_2$  sorption isotherms.  $CO_2$  adsorption isotherm measured at 195 K for a)  $Ti_8Ce_2$ -BA and d)  $Ti_8Ce_2$ -90% BA/10% oFBA, respectively; In-situ differential IR spectra in different range corresponding to the sorption data for b, c)  $Ti_8Ce_2$ -BA and e, f)  $Ti_8Ce_2$ -90% BA/10% oFBA, respectively. Arrows drawn to guide the reader. The IR spectra presented here have been subtracted by the IR spectra of corresponding clusters.

**8**) to obtain the differential spectra. Increases in peak intensities were observed at two regions (3500-3800 cm $^{-1}$  shown in **Figure S8b** and 2100-2500 cm $^{-1}$  shown in **Figure S8c**) as larger amounts of CO $_2$  were dosed. These two regions were then ascribed to the combination bands (3500-3800 cm $^{-1}$ ) of symmetric and asymmetric stretching and the band for asymmetric stretching vibration (2100-2500 cm $^{-1}$ ) of the CO $_2$  molecules that were adsorbed into the cavity of the cluster with weak interactions. Similar cases have been explored previously in the MOFs systems.

To help us gain deeper insights into the  $CO_2$  sorption behavior, the data were separated into three main sections, based on the isotherms. Firstly, we analyze the  $Ti_8Ce_2$ -BA case, as shown in **Figure S31**, which presents the first 16 sorption data points and the corresponding differential IR spectra of  $Ti_8Ce_2$ -BA. Significant, continuous increases are observed in both regions as more  $CO_2$  molecules are being physiosorbed insides the clusters. On the contrary, the differential spectra at the stepped sorption region exhibit

only minor changes not only at the regions of interest discussed above (Figure S32c and S32d), but also the whole range (Figure 8a and S32b, data 16-19). This phenomenon can be attributed to the difference of vibration frequency of CO<sub>2</sub> molecules that interact with Ce sites and being out of the range that the spectra were collected. After the stepped sorption region, the intensities of these bands grow again (Figure S33, data 20-32), indicating that more physiosorbed CO2 molecules are presented inside the cavities. The results suggest that there are three stages for CO2 adsorption on Ti<sub>8</sub>Ce<sub>2</sub>-BA: (1) CO<sub>2</sub> molecules are first physiosorbed in the voids at the initial low-pressure region; (2) as the pressure reaches above 0.3 bar, more CO<sub>2</sub> molecules present close to the Ce sites and form strong interactions, which open the "gate", and (3) thus more CO<sub>2</sub> molecules were adsorbed inside the voids. As such, this result verifies our previous interpretation of the adsorption behavior of Ti<sub>8</sub>Ce<sub>2</sub>-BA (vide supra).

Moreover, we further analyzed the in-situ IR data of Ti<sub>8</sub>Ce<sub>2</sub>-90% BA/10% pFBA (**Figures 8e-f**). We note that the isotherm of Ti<sub>8</sub>Ce<sub>2</sub>-90% BA/10% pFBA in Figure 8d is comparable to the one in Figure 5e but with minor differences that could potentially result from the systematic error from the different measurement settings (see the Experiments Section in SI). The trends in peak intensities within the 3500-3800 cm<sup>-1</sup> and 2100-2500 cm<sup>-1</sup> regions in the spectra (Figures S34, S35, and S36) exhibit similarities to those observed in the Ti<sub>8</sub>Ce<sub>2</sub>-BA case throughout the sorption process. Similarly, it's notable that changes in peak intensities across the entire range of IR spectra are insignificant within the stepped region when compared to the regions before and after the step (as depicted in Figures **8d-8f** and **S35**). The minor changes observed in the stepped region are likely attributed to the concurrent adsorption of physiosorbed CO<sub>2</sub> within voids created by conformational changes induced by the CO<sub>2</sub>-Ce interactions.

To sum up briefly, our observations confirm the  $CO_2$  sorption behavior for  $Ti_8Ce_2$ -90% BA/10% pFBA as follows: (1) Initially, a small amount of  $CO_2$  diffuses into the voids of the clusters during the early stages. (2) Subsequently, conformational changes in the clusters induced by interactions between  $CO_2$  molecules and the Ce sites lead to the creation of space, resulting in observable intensities of physiosorbed  $CO_2$  peaks. (3) Finally, a gradual increase in physiosorbed  $CO_2$  peaks is observed after the stepped region. Overall, the results from in-situ  $CO_2$  isotherms-IR complete the sorption behavior analysis and supplement our theory in understanding the structure-property relationship.

### **SUMMARY**

In summary, we observed a novel and unique stepwisesorption phenomena in a series of bimetallic Ti<sub>8</sub>Ce<sub>2</sub>-oxo clusters, which is the first reported instance in metal oxide Through systematic investigations, clusters. demonstrated that this stepped sorption property is ascribed to CO2-Ce interactions that are heavily affected by the Lewis acidity of the Ce sites and the expansion of lattice voids, which arises from the coordinated ligand conformation variation resulting from the strong interaction formation between the CO<sub>2</sub> molecules and the Ce sites. Moreover, we found that the stepped sorption behavior, including the stepped sorption uptake quantity and gate pressure, can be finely tuned by modulating the

Lewis acidity of Ce sites through the introduction of a second ligand, fluorobenzoic acid, with different amounts and varied F position (e.g., ortho- or para-substituted). A series of in-situ experiments provided insight into the mechanism for "flexibility" of these clusters. For instance, in-situ SCXRD studies confirmed that the accessibility of the Ce site is the main cause strongly influences the stepped sorption behavior, while the introduction of F atoms influence the gate pressure. Detailed sorption profiles for both Ti<sub>8</sub>Ce<sub>2</sub>-BA and Ti<sub>8</sub>Ce<sub>2</sub>-90% BA/10% pFBA were uncovered and completed by in-situ CO2 isotherm-IR analysis. As such, our work reveals the mechanism for the origin of the stepped sorption profile and clearly elucidates the structure-property relationship in these bimetallic metal oxide clusters. Moving forward, these results will contribute to fundamental theories that guide future adsorbent design and profoundly influence future structure-property relationship studies.

### ASSOCIATED CONTENT

# **Supporting Information.**

Additional materials synthesis, characterization, and experimental procedure, including  $CO_2$  isotherms, SEM,  $^1H$  NMR, PXRD, FT-IR, TGA, VT-PXRD, in-situ PXRD, in-situ  $CO_2$  isotherm-IR, etc. This material is available free of charge via the Internet at http://pubs.acs.org."

### **AUTHOR INFORMATION**

### **Corresponding Authors**

- \* Xingjie Wang. State Key Laboratory of Pulp and Paper Engineering, School of Light Industry and Engineering, South China University of Technology, Guangzhou 510640, China; Email: xingjiewang1210@scut.edu.cn
- \* **Susumu Kitagawa**. Institute for Integrated Cell-Material Sciences, Kyoto University, Kyoto, 606-8501 Japan; Email: kitagawa@icems.kyoto-u.ac.jp
- \* Omar K. Farha. Department of Chemistry and International Institute for Nanotechnology, Northwestern University, 2145 Sheridan Road, Evanston, Illinois 60208, United States; Email: o-farha@northwestern.edu

# Notes

The authors declare no competing financial interest.

# ACKNOWLEDGMENT

This work was supported as part of the Northwestern University Institute for Catalysis in Energy Processes (ICEP), funded by the DOE, Office of Basic Energy Sciences (award number DE-FG02-03ER15457) for the cluster preparation and characterizations performed Northwestern University. X.W. gratefully acknowledges support from State Key Laboratory of Pulp and Paper Engineering (202303), Guangzhou Municipal Science and Technology Bureau (no. 2024A04[3650]. acknowledges research support from NSF (CBET 2119433), U.S. Department of Energy (DOE) Office of Science, Basic Energy Sciences Program for separation studies (DE-FG02-08ER15967) for the sorption study of this work, and the Catalyst Design for Decarbonization Center, an Energy Frontier Research Center also funded by the U.S. Department of Energy, Office of Science, Basic Energy Sciences under Award No. DE-SC0023383. F.S. gratefully acknowledges support from the Ryan Fellowship and the International Institute for Nanotechnology at Northwestern University. F.A.S. also acknowledges the Ryan Fellowship and the International Institute for Nanotechnology at Northwestern University along with the Department of Defense (DoD) through the National Defense Science & Engineering Graduate (NDSEG) Fellowship Program. This work made use of the J.B. Cohen X-ray Diffraction Facility supported by the MRSEC program of the National Science Foundation (DMR-1720139) at the Materials Research Center of Northwestern University. This work made use of Keck-II and EPIC facilities of the NUANCE Center at Northwestern University, which has received support from the Soft and Hybrid Nanotechnology Experimental (SHyNE) Resource (NSF NNCI-1542205); the MRSEC program (NSF DMR-1720139) at the Materials Research Center; the International Institute for Nanotechnology (IIN); the Keck Foundation; and the State of Illinois, through the IIN. This work made use of the IMSERC at Northwestern University, which has received support from the NSF (CHE-1048773 and DMR-0521267); SHyNE Resource (NSF NNCI-1542205); the State of Illinois and IIN. This work made use of the IMSERC NMR facility at Northwestern University, which has received support from the Soft and Hybrid Nanotechnology Experimental (SHvNE) Resource (NSF ECCS-2025633), Int. Institute of Nanotechnology, and Northwestern University.

### **REFERENCES**

- (1) Masciocchi, N.; Galli, S.; Colombo, V.; Maspero, A.; Palmisano, G.; Seyyedi, B.; Lamberti, C.; Bordiga, S. Cubic Octanuclear Ni(II) Clusters in Highly Porous Polypyrazolyl-Based Materials. *J. Am. Chem. Soc.* **2010**, *132* (23), 7902-7904. DOI: 10.1021/ja102862j.
- (2) Gao, M.-Y.; Wang, F.; Gu, Z.-G.; Zhang, D.-X.; Zhang, L.; Zhang, J. Fullerene-like Polyoxotitanium Cage with High Solution Stability. *J. Am. Chem. Soc.* **2016**, *138* (8), 2556-2559. DOI: 10.1021/jacs.6b00613.
- (3) Øien-Ødegaard, S.; Bazioti, C.; Redekop, E. A.; Prytz, Ø.; Lillerud, K. P.; Olsbye, U. A Toroidal Zr70 Oxysulfate Cluster and Its Diverse Packing Structures. *Angew. Chem., Int. Ed.* **2020**, *59* (48), 21397-21402. DOI: <a href="https://doi.org/10.1002/anie.202010847">https://doi.org/10.1002/anie.202010847</a> (acccessed 2023/10/05).
- (4) Su, Y.-M.; Wang, Z.; Tung, C.-H.; Sun, D.; Schein, S. Keplerate Ag192 Cluster with 6 Silver and 14 Chalcogenide Octahedral and Tetrahedral Shells. *J. Am. Chem. Soc.* **2021**, *143* (33), 13235-13244. DOI: 10.1021/jacs.1c05664.
- (5) Lv, Y.; Willkomm, J.; Leskes, M.; Steiner, A.; King, T. C.; Gan, L.; Reisner, E.; Wood, P. T.; Wright, D. S. Formation of Ti28Ln Cages, the Highest Nuclearity Polyoxotitanates (Ln=La, Ce). *Eur. J. Chem.* **2012**, *18* (38), 11867-11870. DOI: https://doi.org/10.1002/chem.201201827 (acccessed 2023/10/05).
- (6) Mitchell, K. J.; Abboud, K. A.; Christou, G. Atomically-precise colloidal nanoparticles of cerium dioxide. *Nature Communications* **2017**, *8* (1), 1445. DOI: 10.1038/s41467-017-01672-4.
- (7) Chen, W.-P.; Liao, P.-Q.; Jin, P.-B.; Zhang, L.; Ling, B.-K.; Wang, S.-C.; Chan, Y.-T.; Chen, X.-M.; Zheng, Y.-Z. The Gigantic {Ni36Gd102} Hexagon: A Sulfate-Templated "Star-of-David" for Photocatalytic CO2 Reduction and Magnetic Cooling. *J. Am. Chem. Soc.* **2020**, *142* (10), 4663-4670. DOI: 10.1021/jacs.9b11543.
- (8) Moons, J.; de Azambuja, F.; Mihailovic, J.; Kozma, K.; Smiljanic, K.; Amiri, M.; Cirkovic Velickovic, T.; Nyman, M.; Parac-Vogt, T. N. Discrete Hf18 Metal-oxo Cluster as a Heterogeneous Nanozyme for Site-Specific Proteolysis. *Angew. Chem., Int. Ed.* **2020**, *59* (23), 9094-9101. DOI: <a href="https://doi.org/10.1002/anie.202001036">https://doi.org/10.1002/anie.202001036</a> (acccessed 2023/10/05).
- (9) Russell-Webster, B.; Lopez-Nieto, J.; Abboud, K. A.; Christou, G. Truly Monodisperse Molecular Nanoparticles of Cerium

- Dioxide of 2.4 nm dimensions: A {Ce1000167} Cluster. *Angew. Chem., Int. Ed.* **2021**, *60* (22), 12591-12596. DOI: <a href="https://doi.org/10.1002/anie.202103110">https://doi.org/10.1002/anie.202103110</a> (acccessed 2023/10/05).
- (10) Wang, X.; Brunson, K.; Xie, H.; Colliard, I.; Wasson, M. C.; Gong, X.; Ma, K.; Wu, Y.; Son, F. A.; Idrees, K. B.; et al. Heterometallic CeIV/ VV Oxo Clusters with Adjustable Catalytic Reactivities. *J. Am. Chem. Soc.* **2021**, *143* (49), 21056-21065. DOI: 10.1021/jacs.1c11208.
- (11) Wasson, M. C.; Zhang, X.; Otake, K.-i.; Rosen, A. S.; Alayoglu, S.; Krzyaniak, M. D.; Chen, Z.; Redfern, L. R.; Robison, L.; Son, F. A.; et al. Supramolecular Porous Assemblies of Atomically Precise Catalytically Active Cerium-Based Clusters. *Chem. Mater.*2020, 32 (19), 8522-8529. DOI: 10.1021/acs.chemmater.0c02740.
- (12) Wang, X.; Xie, H.; Knapp, J. G.; Wasson, M. C.; Wu, Y.; Ma, K.; Stone, A. E. B. S.; Krzyaniak, M. D.; Chen, Y.; Zhang, X.; et al. Mechanistic Investigation of Enhanced Catalytic Selectivity toward Alcohol Oxidation with Ce Oxysulfate Clusters. *J. Am. Chem. Soc.* **2022**, *144* (27), 12092-12101. DOI: 10.1021/jacs.2c02625.
- (13) Wasson, M. C.; Wang, X.; Melix, P.; Alayoglu, S.; Wolek, A. T. Y.; Colliard, I.; Son, F. A.; Xie, H.; Weitz, E.; Islamoglu, T.; et al. Interfacial Unit-Dependent Catalytic Activity for CO Oxidation over Cerium Oxysulfate Cluster Assemblies. *ACS Appl. Mater. Interf.* **2022**, *14* (29), 33515-33524. DOI: 10.1021/acsami.2c05937.
- (14) Kitagawa, S.; Kitaura, R.; Noro, S.-i. Functional Porous Coordination Polymers. *Angew. Chem., Int. Ed.* **2004**, *43* (18), 2334-2375. DOI: <a href="https://doi.org/10.1002/anie.200300610">https://doi.org/10.1002/anie.200300610</a> (accessed 2023/12/27).
- (15) Horike, S.; Shimomura, S.; Kitagawa, S. Soft porous crystals. *Nature Chemistry* **2009**, *1* (9), 695-704. DOI: 10.1038/nchem.444.
- (16) Zhao, C.; Han, Y.-Z.; Dai, S.; Chen, X.; Yan, J.; Zhang, W.; Su, H.; Lin, S.; Tang, Z.; Teo, B. K.; et al. Microporous Cyclic Titanium-Oxo Clusters with Labile Surface Ligands. *Angew. Chem., Int. Ed.*2017, 56 (51), 16252-16256. DOI: <a href="https://doi.org/10.1002/anie.201709096">https://doi.org/10.1002/anie.201709096</a> (acccessed 2023/10/05).
- (17) Chen, W.-P.; Liao, P.-Q.; Yu, Y.; Zheng, Z.; Chen, X.-M.; Zheng, Y.-Z. A Mixed-Ligand Approach for a Gigantic and Hollow Heterometallic Cage {Ni64RE96} for Gas Separation and Magnetic Cooling Applications. *Angew. Chem., Int. Ed.* **2016**, *55* (32), 9375-9379. DOI: <a href="https://doi.org/10.1002/anie.201603907">https://doi.org/10.1002/anie.201603907</a> (acccessed

- 2023/10/05).
- (18) Hong, K.; Chun, H. Nonporous Titanium–Oxo Molecular Clusters That Reversibly and Selectively Adsorb Carbon Dioxide. *Inorg. Chem.* **2013**, *52* (17), 9705-9707. DOI: 10.1021/ic401122u.
- (19) Hong, K.; Bak, W.; Chun, H. Robust Molecular Crystals of Titanium(IV)-oxo-Carboxylate Clusters Showing Water Stability and CO2 Sorption Capability. *Inorg. Chem.* **2014**, *53* (14), 7288-7293. DOI: 10.1021/ic500629y.
- (20) Yuan, S.; Qin, J.-S.; Xu, H.-Q.; Su, J.; Rossi, D.; Chen, Y.; Zhang, L.; Lollar, C.; Wang, Q.; Jiang, H.-L.; et al. [Ti8Zr2012(C00)16] Cluster: An Ideal Inorganic Building Unit for Photoactive Metal-Organic Frameworks. *ACS Cent. Sci.* **2018**, *4* (1), 105-111. DOI: 10.1021/acscentsci.7b00497.
- (21) Shah, P.; Westwell, A. D. The role of fluorine in medicinal chemistry. *J Enzyme Inhib Med Chem* **2007**, *22* (5), 527-540. DOI: 10.1080/14756360701425014 From NLM.
- (22) Gillis, E. P.; Eastman, K. J.; Hill, M. D.; Donnelly, D. J.; Meanwell, N. A. Applications of Fluorine in Medicinal Chemistry. *Journal of Medicinal Chemistry* **2015**, *58* (21), 8315-8359. DOI: 10.1021/acs.jmedchem.5b00258.
- (23) Meanwell, N. A. Fluorine and Fluorinated Motifs in the Design and Application of Bioisosteres for Drug Design. *Journal of Medicinal Chemistry* **2018**, *61* (14), 5822-5880. DOI: 10.1021/acs.jmedchem.7b01788.
- (24) Xie, H.; Vignesh, K. R.; Zhang, X.; Dunbar, K. R. From spin-crossover to single molecule magnetism: tuning magnetic properties of Co(ii) bis-ferrocenylterpy cations via supramolecular interactions with organocyanide radical anions. *Journal of Materials Chemistry C* **2020**, *8* (24), 8135-8144, 10.1039/D0TC00830C. DOI: 10.1039/D0TC00830C.
- (25) TiCe Oxo Cluster for Photocatalytic Oxidation. Submitted.
- (26) Duan, J.; Higuchi, M.; Foo, M. L.; Horike, S.; Rao, K. P.; Kitagawa, S. A Family of Rare Earth Porous Coordination Polymers with Different Flexibility for CO2/C2H4 and CO2/C2H6 Separation. *Inorg. Chem.* **2013**, *52* (14), 8244-8249. DOI: 10.1021/ic401157n.
- (27) Kanoo, P.; Matsuda, R.; Sato, H.; Li, L.; Hosono, N.; Kitagawa, S. Pseudo-Gated Adsorption with Negligible Volume Change Evoked by Halogen-Bond Interaction in the Nanospace of MOFs. *Eur. J. Chem.* **2020**, *26* (10), 2148-2153. DOI: <a href="https://doi.org/10.1002/chem.201904703">https://doi.org/10.1002/chem.201904703</a> (acccessed 2023/10/05).
- (28) Yao, X.; Cordova, K. E.; Zhang, Y.-B. Flexible Metal-Organic Frameworks as CO2 Adsorbents en Route to Energy-Efficient Carbon Capture. *Small Structures* **2022**, *3* (5), 2100209. DOI:

https://doi.org/10.1002/sstr.202100209 2023/10/05). (acccessed

- (29) Walton, K. S.; Millward, A. R.; Dubbeldam, D.; Frost, H.; Low, J. J.; Yaghi, O. M.; Snurr, R. Q. Understanding Inflections and Steps in Carbon Dioxide Adsorption Isotherms in Metal-Organic Frameworks. *J. Am. Chem. Soc.* **2008**, *130* (2), 406-407. DOI: 10.1021/ja076595g.
- (30) Kang, C.; Zhang, Z.; Usadi, A. K.; Calabro, D. C.; Baugh, L. S.; Chai, K.; Wang, Y.; Zhao, D. Tunable Interlayer Shifting in Two-Dimensional Covalent Organic Frameworks Triggered by CO2 Sorption. *J. Am. Chem. Soc.* **2022**, *144* (44), 20363-20371. DOI: 10.1021/jacs.2c08214.
- (31) Kang, C.; Zhang, Z.; Kusaka, S.; Negita, K.; Usadi, A. K.; Calabro, D. C.; Baugh, L. S.; Wang, Y.; Zou, X.; Huang, Z.; et al. Covalent organic framework atropisomers with multiple gastriggered structural flexibilities. *Nature Materials* **2023**, *22* (5), 636-643. DOI: 10.1038/s41563-023-01523-2.
- (32) Wang, H.; Li, B.; Wu, H.; Hu, T.-L.; Yao, Z.; Zhou, W.; Xiang, S.; Chen, B. A Flexible Microporous Hydrogen-Bonded Organic Framework for Gas Sorption and Separation. *J. Am. Chem. Soc.* **2015**, *137* (31), 9963-9970. DOI: 10.1021/jacs.5b05644.
- (33) Hisaki, I.; Nakagawa, S.; Suzuki, Y.; Tohnai, N. CO2 Sorption of Layered Hydrogen-bonded Organic Framework Causes Reversible Structural Changes Involving Four Different Crystalline States under Ambient Pressure. *Chemistry Letters* **2018**, *47* (9), 1143-1146. DOI: 10.1246/cl.180491 (acccessed 2023/10/05).
- (34) Huang, Q.; Li, W.; Mao, Z.; Qu, L.; Li, Y.; Zhang, H.; Yu, T.; Yang, Z.; Zhao, J.; Zhang, Y.; et al. An exceptionally flexible hydrogen-bonded organic framework with large-scale void regulation and adaptive guest accommodation abilities. *Nature Communications* **2019**, *10* (1), 3074. DOI: 10.1038/s41467-019-10575-5.
- (35) Zhang, Z.; Peh, S. B.; Krishna, R.; Kang, C.; Chai, K.; Wang, Y.; Shi, D.; Zhao, D. Optimal Pore Chemistry in an Ultramicroporous Metal-Organic Framework for Benchmark Inverse CO2/C2H2 Separation. *Angew. Chem., Int. Ed.* **2021**, *60* (31), 17198-17204. DOI: <a href="https://doi.org/10.1002/anie.202106769">https://doi.org/10.1002/anie.202106769</a> (acccessed 2023/10/05).
- (36) Cavallo, M.; Atzori, C.; Signorile, M.; Costantino, F.; Venturi, D. M.; Koutsianos, A.; Lomachenko, K. A.; Calucci, L.; Martini, F.; Giovanelli, A.; et al. Cooperative CO2 adsorption mechanism in a perfluorinated CeIV-based metal organic framework. *J. Mater. Chem. A* **2023**, *11* (11), 5568-5583, 10.1039/D2TA09746J. DOI: 10.1039/D2TA09746J.
- (37) Braude, E. A., Nachod, F.C.. Determination of Organic

- Structures by Physical Methods; Academic Press, 1955.
- (38) Rayder, T. M.; Formalik, F.; Vornholt, S. M.; Frank, H.; Lee, S.; Alzayer, M.; Chen, Z.; Sengupta, D.; Islamoglu, T.; Paesani, F.; et al. Unveiling Unexpected Modulator-CO2 Dynamics within a Zirconium Metal-Organic Framework. *J. Am. Chem. Soc.* **2023**, *145* (20), 11195-11205. DOI: 10.1021/jacs.3c01146.
- (39) Bordiga, S.; Regli, L.; Bonino, F.; Groppo, E.; Lamberti, C.; Xiao, B.; Wheatley, P. S.; Morris, R. E.; Zecchina, A. Adsorption properties of HKUST-1 toward hydrogen and other small molecules monitored by IR. *Phys. Chem. Chem. Phys.* **2007**, *9* (21), 2676-2685, 10.1039/B703643D. DOI: 10.1039/B703643D.
- (40) Dietzel, P. D. C.; Johnsen, R. E.; Fjellvåg, H.; Bordiga, S.; Groppo, E.; Chavan, S.; Blom, R. Adsorption properties and structure of CO2 adsorbed on open coordination sites of metalorganic framework Ni2(dhtp) from gas adsorption, IR spectroscopy and X-ray diffraction. *Chemical Communications* **2008**, (41), 5125-5127, 10.1039/B810574J. DOI: 10.1039/B810574J.